Comparison of the temperature-dependent electronic structure of the perovskites $La_{0.65}A_{0.35}MnO_3$ (A=Ca,Ba)

D. N. McIlroy,* C. Waldfried, Jiandi Zhang,† J.-W. Choi, F. Foong, S. H. Liou, and P. A. Dowben
The Department of Physics and Astronomy and the Center for Materials Research and Development, Behlen Laboratory, The University of Nebraska–Lincoln, Lincoln, Nebraska 68588-0111
(Received 11 June 1996)

The electronic band structure and the local screening effects of the transition-metal perovskites $La_{0.65}A_{0.35}MnO_3$ (A=Ba and Ca) have been examined across the coupled magnetic-metallic phase transition using the techniques of angle-resolved photoemission, resonance photoemission, and inverse photoemission. Temperature-dependent band shifts of the e_g and t_{2g} bands of $La_{0.65}Ca_{0.35}MnO_3$ have been observed. These changes in the observed electronic structure correlate with the phase transition, and are in qualitatively agreement with the predicted behavior associated with double exchange coupled with a dynamic Jahn-Teller distortion. Similar shifts were not observed for $La_{0.65}Ba_{0.35}MnO_3$. The changes in local screening across the Curie temperature were substantially larger for $La_{0.65}Ca_{0.35}MnO_3$ than for $La_{0.65}Ba_{0.35}MnO_3$. This is consistent with the less itinerant band structure of $La_{0.65}Ca_{0.35}MnO_3$, as compared to the highly dispersive bands of $La_{0.65}Ba_{0.35}MnO_3$. These results suggest that there is less hybridization in $La_{0.65}Ca_{0.35}MnO_3$, as compared to $La_{0.65}Ba_{0.35}MnO_3$. The results point to greater electron localization in the $La_{0.65}Ca_{0.35}MnO_3$ compound. [S0163-1829(96)05048-5]

I. INTRODUCTION

Lanthanum-based transition-metal oxide perovskites are experiencing a revival in interest. This renewed interest has been driven by the discovery and subsequent studies of their ''colossal'' magnetoresistance (CMR) behavior.[1–11] The family of $La_{1-x}A_xMnO_3$ (A= Ca, Sr, and Ba) perovskites are unique in that they are antiferromagnetic insulators for the parent compounds, and ferromagnetic metals for intermediate concentrations below some critical temperature T_c. The doping regime for achieving CMR typically occurs in the range of $0.2 \leqslant x \leqslant 0.5$.

Based on the initial magnetic and transport experiments on the doped phases of $La_{1-x}A_xMnO_3$ (A= Ca, Sr, and Ba) by van Santen and Jonker,[12,13] Zener[14] developed a double-exchange model to explain these systems. In this model, transport is achieved through the simultaneous hopping of electrons between Mn ions (Mn^{3+} and Mn^{4+}) and O ion, with the restriction that the two electrons have the same spin and that the moments of the two Mn ions are parallel. The role of doping is to change the valency of the Mn ions from Mn^{3+} to a mixed phase of Mn^{3+} and Mn^{4+}. There are three electrons in the t_{2g} band and one in the e_g band associated with the Mn^{3+} ions, while the e_g band is empty for the Mn^{4+} ions. Conduction is achieved through the hopping of an electron in the e_g state of the Mn^{3+} ions into the unoccupied e_g band of the Mn^{4+} ions. This model connects the necessity for magnetic order to metallic transport, and, with the inclusion of magnetic polarons, this model has achieved wide acceptance. It accounts for both the magnetic frustration for $T > T_c$ and the turnaround in the resistivity in the semiconducting phase once a maximum in the resistivity has occurred.

While at first glance this model provides an acceptable explanation for the CMR phenomena, reexamination of the double exchange mechanism has shown that it is insufficient by itself to drive these systems from their metallic/ferromagnetic phases into a semiconducting-paramagnetic phase.[15] Millis, Littlewood, and Shraiman[15] instead suggested that strong electron-phonon interactions are present, which drive the systems through dynamic Jahn-Teller distortions. Indeed, temperature-dependent neutron powder diffraction experiments on $La_{0.65}Ca_{0.35}MnO_3$ (Refs. 16 and 17) have identified Jahn-Teller distortions correlated with the coupled metallic-magnetic transition ($T_c \sim 240$ K). While neutron-diffraction measurements clearly demonstrate that a dynamic Jahn-Teller distortion occurs for $La_{0.65}Ca_{0.35}MnO_3$,[17] $La_{0.65}Ba_{0.35}MnO_3$ may be fundamentally different. $La_{0.65}Sr_{0.35}MnO_3$, which should more closely resemble $La_{0.65}Ba_{0.35}MnO_3$ than $La_{0.65}Ca_{0.35}MnO_3$, does not exhibit anomalous behavior in the rms motion of the oxygen atoms near T_c.[18]

While, to our knowledge, no evidence as yet exists which demonstrates the absence of large dynamic Jahn-Teller distortions in $La_{0.65}Ba_{0.35}MnO_3$, other differences may exist in this material, as suggested by studies of the close cousin $La_{0.65}Sr_{0.35}MnO_3$. In $La_{0.65}Sr_{0.35}MnO_3$,[7] the ferromagnetic Curie temperature is *not* accompanied by a metal-to-nonmetal transition, in spite of the presence of substantial magnetoresistance. The fundamental issue of whether differences in the electronic structures between Sr-, Ba-, and Ca-doped transition-metal perovskites can lead to a coupled ferromagnetic-paramagnetic–metal-nonmetal transition in the latter and only a ferromagnetic-paramagnetic transition in the former, is critical toward increasing our fundamental understanding of these materials.

There is strong evidence that volumetric changes modify the coupled transition of $La_{0.7-x}Y_xCa_{0.30}MnO_3$ ($0 \leqslant x \leqslant 0.25$).[19,20] It has been shown that the transition temperature of the coupled transition of $La_{0.7-x}Y_xCa_{0.30}MnO_3$

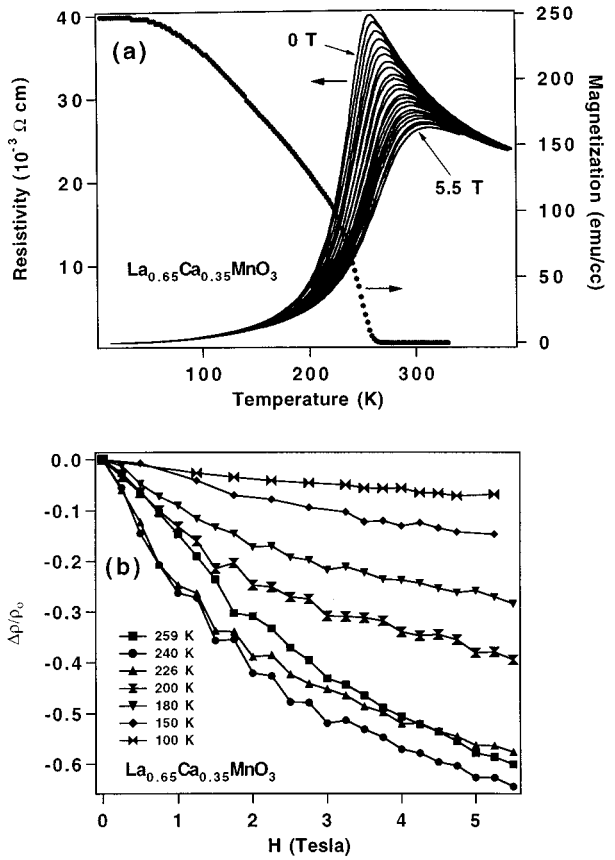

FIG. 1. (a) The bulk resistivity (solid lines) of $La_{0.65}Ca_{0.35}MnO_3$, acquired in applied fields ranging from 0 to 5.5 T in 0.25-T steps, and the bulk magnetization in an in-plane applied field of 50 G (●), both as a function of temperature. (b) The field-dependent resistivity isotherms of resistivity curves in (a).

can be shifted by changing the Y doping concentration. This behavior has been interpreted in terms of band tuning, which modifies the indirect coupling between the Mn ions.[19,20] This type of lattice tuning should also occur for different dopants, i.e., Ca versus Ba, for example. If this is indeed the case, such changes in the band structure should be observed with angle-resolved photoemission.

At issue is electronic screening and how it may differ from system to system. What role does screening, and by extension metallicity, play in these systems? With sufficient screening parameter, are dynamic Jahn-Teller distortions suppressed? In order to help address these issues we have examined the temperature dependence of the electronic structure of $La_{0.65}Ca_{0.35}MnO_3$ and $La_{0.65}Ba_{0.35}MnO_3$ using angle-resolved ultraviolet photoemission spectroscopy (ARUPS), constant-initial-state spectroscopy (CIS), and inverse photoemission electron spectroscopy (IPES). The simplicity of comparing these two materials with equivalent doping concentrations should demonstrate that changes in the electronic structure are due to lattice changes arising from the different ionic radii of the dopants, and, ultimately, to changes in hybridization.

II. SAMPLE PREPARATION AND EXPERIMENTAL DETAILS

The samples were grown on (100) $LaAlO_3$ substrates by rf sputtering. The nominal target concentrations were

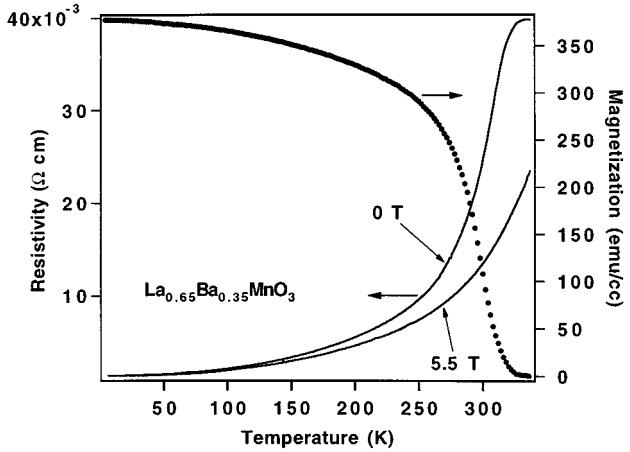

FIG. 2. The bulk resistivity (solid lines) of $La_{0.65}Ba_{0.35}MnO_3$, acquired in applied fields of 0 and 5.5 T, and the bulk magnetization in an in-plane applied field of 50 G (●), both as a function of temperature.

$La_{0.65}Ca_{0.35}MnO_x$ and $La_{0.65}Ba_{0.35}MnO_x$. The samples were grown in a 2:1 argon/oxygen atmosphere maintained at 20 m Torr, with the substrate maintained at a temperature of 700 °C throughout the growth process. The films were subsequently annealed at 900 °C in an oxygen atmosphere maintained at a pressure of 2 atm for 10 h. This final procedure was found to improve the compositional homogeneity of the samples. The chemical composition of the films was determined from energy dispersive x-ray spectroscopy, and found to be similar to the targets with final compositions: $La_{0.65}Ca_{0.35}MnO_3$ and $La_{0.65}Ba_{0.35}MnO_3$. The thicknesses of the $La_{0.65}Ca_{0.35}MnO_3$ and $La_{0.65}Ba_{0.35}MnO_3$ samples were nominally 2500 and 1500 Å, respectively. Based on room-temperature x-ray diffraction studies, the samples were determined to be crystalline and single domained.

The sample quality was additionally verified from the measured magnetization, resistivity, and the field-dependent resistivity ($\Delta\rho/\rho_O$). In Fig. 1(a) we present the resistivity of $La_{0.65}Ca_{0.35}MnO_3$ in a zero field and for various magnetic fields up to 5.5 T as a function of temperature. The magnetization is also included in Fig. 1(a). For this sample the critical temperature (T_c) is 260 K. The isotherms of the field dependence of the resistivity of this sample are displayed in Fig. 1(b), and are characteristic of a well-ordered $La_{0.65}Ca_{0.35}MnO_3$ sample.[6] The resistivity and magnetization measurements of the $La_{0.65}Ba_{0.35}MnO_3$ sample are displayed in Fig. 2, from which we determined a T_c of 330 K. The behavior of the magnetoresistance isotherms of this sample were similar to those displayed in Fig. 1(b).

The magnetization and the temperature dependent resistivity were measured using a superconducting quantum interference device magnetometer and a four-point probe, respectively. The magnetic measurements were obtained with an in-plane magnetic field of 50 G. The samples exhibited the characteristic giant magnetoresistance expected of these doped transition-metal oxides (see Figs. 1 and 2).

The angle-resolved photoemission spectroscopy and the constant-initial-state spectroscopy experiments on $La_{0.65}Ca_{0.35}MnO_3$ were performed using synchrotron radiation dispersed by a 6-m monochromator, while a 3-m toroidal grating monochromator was used to disperse the syn-

chrotron radiation in the $La_{0.65}Ba_{0.35}MnO_3$ studies. Both of these experiments were conducted at the Synchrotron Radiation Center in Stoughton, Wl, and are discussed in detail elsewhere.[21] The ultrahigh-vacuum chamber was maintained at a base pressure between $6-8\times10^{-11}$ Torr, and was equipped with an angle-resolved electron analyzer with an acceptance angle of $\pm1°$. The combined energy resolution of the analyzer and the light source was about 150 meV or less. The chamber was also equipped with a low-energy electron-diffraction (LEED) system for establishing long-range surface crystallographic order. The work presented here was undertaken with a light incidence angle of 45° for $La_{0.65}Ca_{0.35}MnO_3$ ($s+p$-polarized light) and 65° for $La_{0.65}Ba_{0.35}MnO_3$ (p-polarized light). Throughout this work, the component of the vector potential A, in the plane of the surface, is in the plane defined by the surface normal and the detector (even geometry), i.e., parallel to the $\overline{\Gamma}$-$\overline{X}$ direction.

The inverse photoemission electron spectroscopy spectra of both $La_{0.65}Ca_{0.35}MnO_3$ and $La_{0.65}Ba_{0.35}MnO_3$ were acquired in an UHV chamber with a base pressure of 1×10^{-10} Torr. The IPES measurements were performed in an isochromatic mode, where 9.8-eV photons were detected with a Geiger-Muller tube equipped with a CaF_2 window. The low-energy electrostatic gun used was based on the Zipf design[22] with a BaO cathode. The electron-beam divergence was better than 3°, resulting in an uncertainty of the wave vector $k_\parallel$ of about $\Delta k_\parallel = 0.06$ Å^{-1}. By characterizing the elastically scattered electron beam off of a copper single crystal using a large hemispherical analyzer, the average full width at half maximum of the specular beam was determined to be better than 350 meV. Upon examination of the Fermi level of a clean Cu(100) crystal, the overall resolution was found to be better than 400 meV. At no time during IPES acquisition were effects due to sample charging observed. In addition to IPES, the chamber was equipped with LEED, x-ray photoemission spectroscopy (XPS), and ultraviolet photoemission spectroscopy (UPS) using a helium discharge lamp. The LEED pattern and the UPS spectra were equivalent to those obtained in the ARUPS system, and verified the equivalency of the sample surfaces for both the $La_{0.65}Ca_{0.35}MnO_3$ and $La_{0.65}Ba_{0.35}MnO_3$ samples.

III. SURFACE PREPARATION

Upon insertion into the ARUPS UHV chamber and the IPES UHV chamber, the $La_{0.65}Ca_{0.35}MnO_3$ sample was annealed at 450 °C, and periodically annealed thereafter. Low-energy electron-diffraction measurements indicated that the surface was well ordered with a cubic structure (see Fig. 3). These LEED patterns are consistent with LEED patterns of the (100) surfaces of $SrTiO_3$.[23] The LEED structures of $La_{0.65}Ca_{0.35}MnO_3$ and $La_{0.65}Ba_{0.35}MnO_3$ in Fig. 3 demonstrate that there is preferential film growth along the (100) direction. The annealing maintained a clean surface free of contamination. The $La_{0.65}Ba_{0.35}MnO_3$ samples were also annealed, but additional steps, which will be discussed in Sec. IV were undertaken to clean the surface. Both x-ray diffraction and LEED are consistent with a surface unit cell of 5.56 Å.

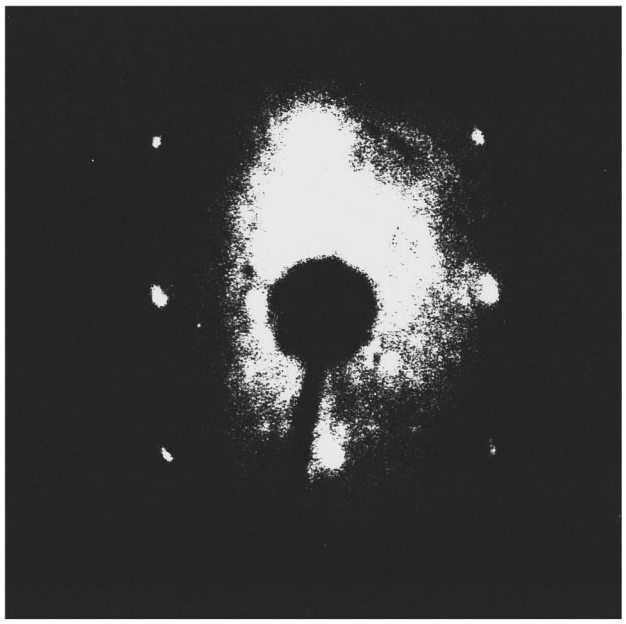

(a)

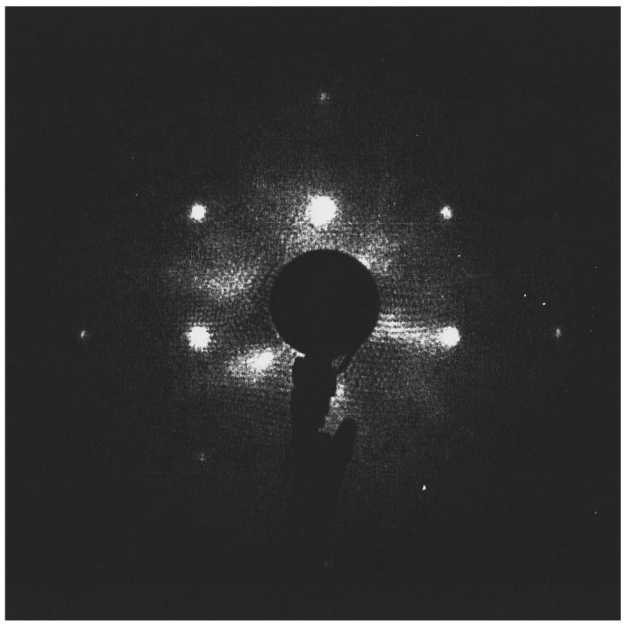

(b)

FIG. 3. The low-energy electron-diffraction pattern of (a) $La_{0.65}Ca_{0.35}MnO_3$ acquired at room temperature with an electron incidence energy of 66.4 eV and (b) $La_{0.65}Ba_{0.35}MnO_3$, acquired at room temperature with an electron incidence energy of 62.5 eV.

IV. RESULTS

A. Surface properties

The surface of $La_{0.65}Ca_{0.35}MnO_3$ is fairly inert, and is not prone to surface contamination, as determined by XPS and ARUPS. In contrast, the surface of $La_{0.65}Ba_{0.35}MnO_3$ was found to be much more reactive. The bottom photoemission spectrum in Fig. 4 is for a contaminated $La_{0.65}Ba_{0.35}MnO_3$ surface. Three features in the valence band have been identified as the 5σ (6eV), 1π (8eV), and 4σ (12eV, partially displayed in Fig. 4) molecular orbitals of CO.[24] The molecular adsorption of CO on transition-metal oxides has previ-

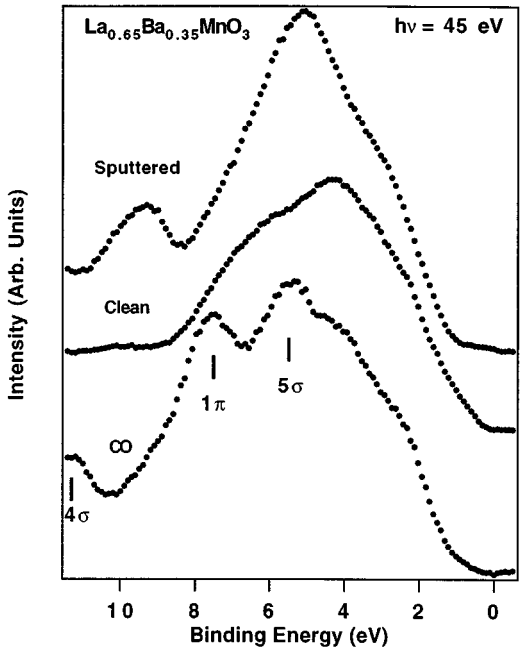

FIG. 4. Valence-band spectra of $La_{0.65}Ba_{0.35}MnO_3$ for a sputtered surface (top), clean (center), and with CO adsorption. The spectra were acquired at room temperature at normal emission with a photon energy of 45 eV.

ously been observed for MnO.[25] Annealing at 450 °C was found to remove the majority of surface contamination. A very clean surface was obtained by exposing the sample at room temperature to zero-order light from the synchrotron for 30 min, at which point no evidence of molecular CO was detected. The clean photoemission spectrum of $La_{0.65}Ba_{0.35}MnO_3$ is displayed in Fig. 4. We postulate that CO is removed by low-energy electron-stimulated desorption, since a large number of low-energy secondary electrons are generated upon exposure to zero-order light.

We are confident that the CO molecules do not photodissociate, and leave carbon behind as there was no detectable carbon 1*s* core-level signal observed with XPS. In addition, the density of states near the Fermi level is very sensitive to surface contamination and surface order (to be discussed below, as well as in Ref. 26). We believe that photon-induced damage does not occur during the cleaning process with zero-order light, since the sputtered surface (Fig. 4) demonstrates that surface damage (defects) will greatly reduce the density of states and the concomitant photoemission signal near the Fermi level, i.e., in the region between 0 and 2-eV binding energies. The cleaning technique using zero-order light was also found to work quite well for some high-temperature superconductors.

Carbon monoxide contamination could also be observed in the IPES spectra of $La_{0.65}Ba_{0.35}MnO_3$. In Fig. 5 we display a clean IPES spectrum of $La_{0.65}Ba_{0.35}MnO_3$, and one with CO surface contamination. A comparison of the two spectra illustrate the suppression of the density of states at the Fermi level. The feature at 4.0 eV above the Fermi level in Fig. 5 is the $2\pi^*$ antibonding molecular orbital of CO.[27–29]

In order to determine the effects of disorder on the electronic structure of $La_{0.65}Ba_{0.35}MnO_3$, as well as other perovskites, the surface was sputtered for 10 min in a 1-keV

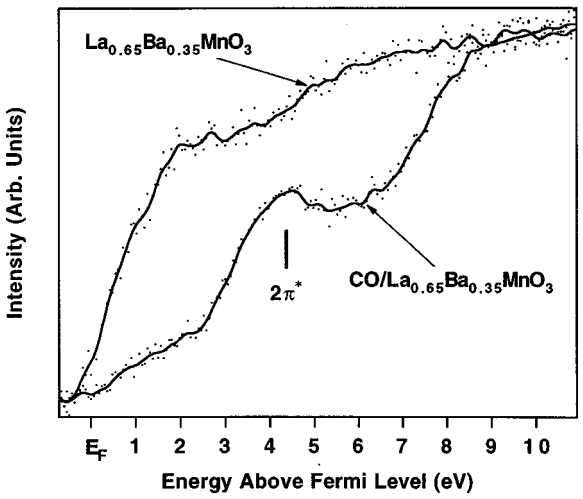

FIG. 5. Inverse-photoemission spectra of a clean surface of $La_{0.65}Ba_{0.35}MnO_3$ (top) and with CO adsorption (bottom).

Ar^+-ion beam. A spectrum of the sputtered surface is displayed in Fig. 4. Both the suppression and the introduction of states is observed with sputtering. An examination of the sputtered valence-band spectrum in Fig. 4 reveals the strong suppression of the density of states from the Fermi level down to approximately 1.75-eV binding energy. The intensity of a state at approximately 3.35 eV also decreases with sputtering. The intensity of these same states were also seen to decrease with CO adsorption. There is a similar suppression of states just above the Fermi energy seen in inverse photoemission. The implications of these results will be discussed in detail in Sec. V.

While some of the valence-band states are suppressed with sputtering, others are seen to increase in intensity and dominate the valence spectrum. The intensity of the oxygen 2*p*-derived state at 6 eV increases with sputtering, and dominates the valence band, and a state at 10 eV is also observed. In addition to the above modifications of the valence band of $La_{0.65}Ba_{0.35}MnO_3$ with sputtering, the disordered surface exhibited little or no dispersion.

B. Photoemission, inverse photoemission, and constant-initial-state spectroscopy of $La_{0.65}Ca_{0.35}MnO_3$ and $La_{0.65}Ba_{0.35}MnO_3$

1. $La_{0.65}Ca_{0.35}MnO_3$

In Fig. 6(a) we present the photon energy dependence of $La_{0.65}Ca_{0.35}MnO_3$ at room temperature. It is clear from Fig. 6(a) that there is very little dispersion perpendicular to the surface. The state at a binding energy of 7.8 eV disperses by only 200 meV at best, and the other valence-band features by even less. The lack of perpendicular dispersion is not an indication that the valence-band states are surface states, but merely that the states are localized.

In Fig. 7, we present the valence-band spectra of $La_{0.65}Ca_{0.35}MnO_3$ for a variety of electron emission angles along the $\overline{\Gamma}$-X high-symmetry direction. The line-shape analysis of the energy distribution curves of $La_{0.65}Ca_{0.35}MnO_3$ is displayed in the bottom spectrum of Fig. 7. While we have chosen to use six peaks to analyze the

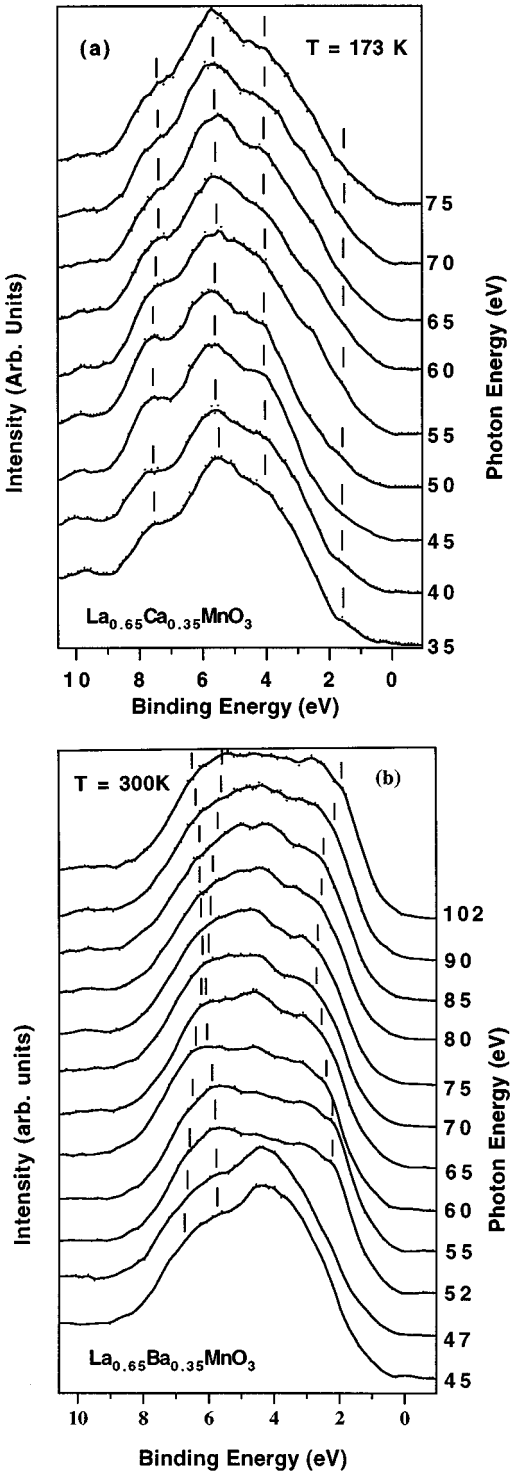

FIG. 6. The photon energy dependence of the valence band at normal emission of (a) $La_{0.65}Ca_{0.35}MnO_3$ and (b) $La_{0.65}Ba_{0.35}MnO_3$.

spectra, we cannot and do not disregard the possibility that more bands exist. Based on the line-shape analysis of the valence band, for both low temperature (173 K) and room temperature, we have determined the dispersion of the $La_{0.65}Ca_{0.35}MnO_3$ states, which is presented in Fig. 8. Similar to the $k_\perp$ dispersion, the $k_\parallel$ dispersion is also very flat with bandwidths $\leqslant 200$ meV. These results indicate that the occupied states of $La_{0.65}Ca_{0.35}MnO_3$ are extremely localized, both

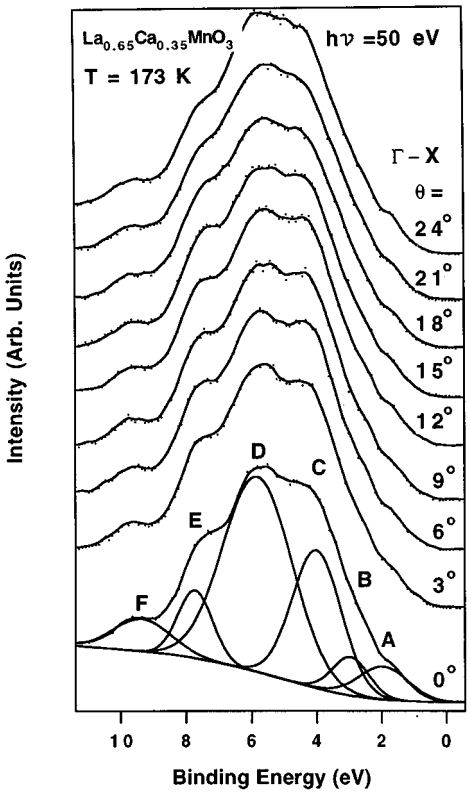

FIG. 7. Valence-band spectra of $La_{0.65}Ca_{0.35}MnO_3$ acquired at a photon energy of 50 eV along the Γ-X high-symmetry direction. The bottom spectrum has been deconvoluted with an integrated background into six components labeled A–F, respectively.

in $k_\parallel$ and perpendicular to the surface plane ($k_\perp$).

There is a distinct increase in the spectral weight in the region between the Fermi level and 3 eV in the valence-band spectrum in Fig. 6, as the photon energy is increased from 45 to 50 eV. This resonance in the photoemission occurs when the photon energy is swept through the $3p$ Mn adsorption edge.[30] Ionization of the excited $3p^5 3d^{n+1}$ state yields a final state $3p^6 3d^{n-1} + e^-$, which is identical with the direct

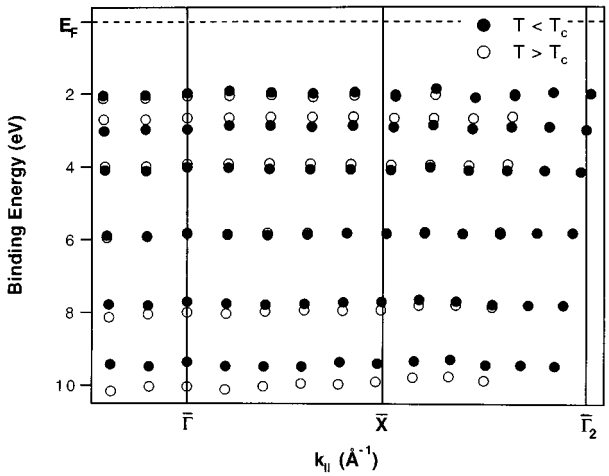

FIG. 8. The measured band structure of the six bands of $La_{0.65}Ca_{0.35}MnO_3$ in Fig. 7 along the Γ-X high symmetry direction, both above (O) and below (●) T_c ($\simeq 260$ K).

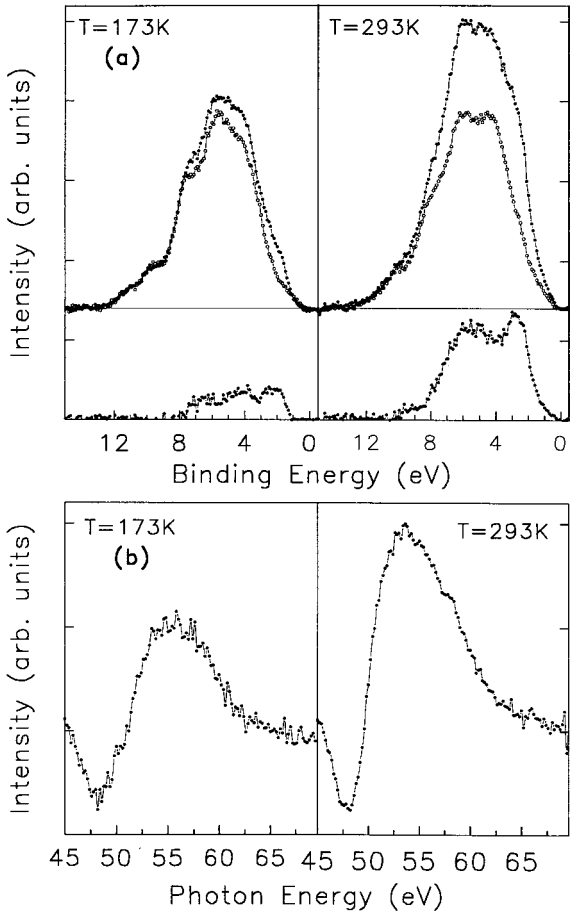

FIG. 9. (a) Valence-band spectra of $La_{0.65}Ca_{0.35}MnO_3$ acquired with photon energies of 55 eV (●) and 47 eV (O) at 173 K ($<T_c$) and 293 K ($>T_c$). The difference curves for the two spectra acquired with different photon energies, but at the same temperature, are displayed below the respective valence spectra. (b) The resonance photoemission spectra of $La_{0.65}Ca_{0.35}MnO_3$ at 173 and 293 K, respectively, where the initial state is at a binding energy of 2.7 eV.

valence-band excitation. The resonance effect can be summarized as follows:

$$h\nu + 3p^6d^n \rightarrow 3p^5d^{n+1} \rightarrow 3p^6 3d^{n-1} + e^-.$$

An example of this enhancement of the valence band of $La_{0.65}Ca_{0.35}MnO_3$ is displayed in panel (a) of Fig. 9. The increase in the photoemission intensity identifies the bands with Mn $3d$ character. The resonant enhancement of the valence band of $La_{0.65}Ca_{0.35}MnO_3$ in Fig. 9 extends from the Fermi level down to a binding energy of 8 eV. Similar resonances have been observed for $SrMnO_3$ and $LaMnO_3$.[31]

The resonance process can be probed using the technique of constant-initial-state spectroscopy. In CIS, the intensity of an initial state is characterized as a function of the photon energy. This reflects the change in the partial cross section of the direct photoemission process, as well as the indirect process discussed above. The CIS spectra, or resonance photoemission spectra, of $La_{0.65}Ca_{0.35}MnO_3$ are displayed in panel (b) of Fig. 9. A distinct threshold occurs at a photon energy of 47 eV, as expected, with a maximum intensity at 54 eV.

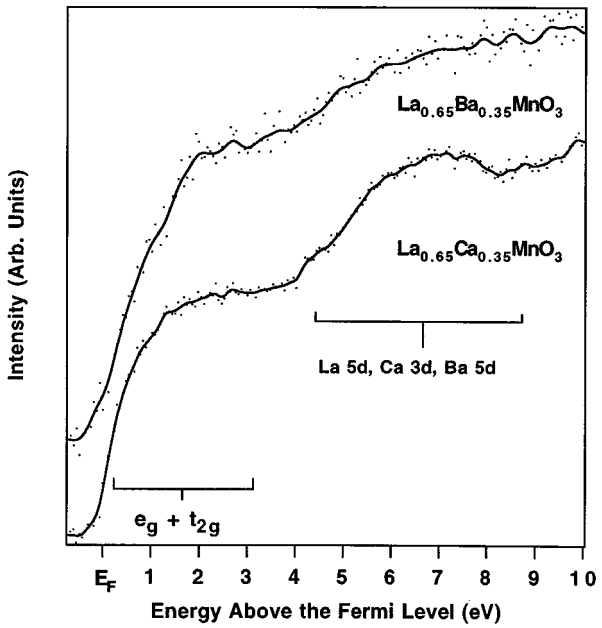

FIG. 10. Inverse-photoemission spectra of the clean surfaces of $La_{0.65}Ba_{0.35}MnO_3$ (top) and $La_{0.65}Ca_{0.35}MnO_3$ (bottom).

The structure of the CIS spectra of $La_{0.65}Ca_{0.35}MnO_3$ are similar to those obtained for MnO by Lad and Henrich.[32]

A characteristic IPES spectrum of $La_{0.65}Ca_{0.35}MnO_3$ is presented in Fig. 10. Due to the highly hybridized nature of the Mn $3d$–O $2p$ bands and the lower resolution of the IPES system, the spectrum does not exhibit the type of well-pronounced structure observed for metals. Our IPES spectrum is similar to bremsstrahlung isochromatic spectroscopy work on $La_{1-x}Sr_xMnO_3$ by Chainani, Mathew, and Sarma.[33] The IPES spectrum in Fig. 10, in conjunction with the UPS spectrum in Fig. 7 suggests, as in the case of the work from other groups[34] (ignoring all the complications of final-state effects), that there is a gap in this system or at least a low density of occupied states at the Fermi level.

2. $La_{0.65}Ba_{0.35}MnO_3$

In Fig. 6(b) the photon energy dependence of the valence band of $La_{0.65}Ba_{0.35}MnO_3$ is presented. The tick marks indicate the binding-energy positions of three bands which disperse with changes in photon energy. The $k_\perp$ dependence of these states indicates that these states have bulk character. The two bands at binding energies of 1.6 and 3.35 eV in Fig. 6(b) do not disperse with changes in photon energy. This indicates that these two bands are either highly localized, or are restricted to the surface, and therefore do not have a perpendicular component of momentum.

In Fig. 11 a series of spectra of $La_{0.65}Ba_{0.35}MnO_3$ acquired at different emission angles, i.e., for different values of $k_\parallel$, are displayed. An examination of Fig. 11 reveals the rich in-plane dispersive behavior of the $La_{0.65}Ba_{0.35}MnO_3$ bands along the Γ-X high-symmetry direction. In Fig. 12 we plot the intensity of the 3.35-eV band as a function of emission angle for photon energies of 45, 55, and 65 eV. A systematic increase in the intensity of this band occurs in either direction away from normal emission, except for the spectra acquired with a photon energy of 45 eV (below the Mn $3p$

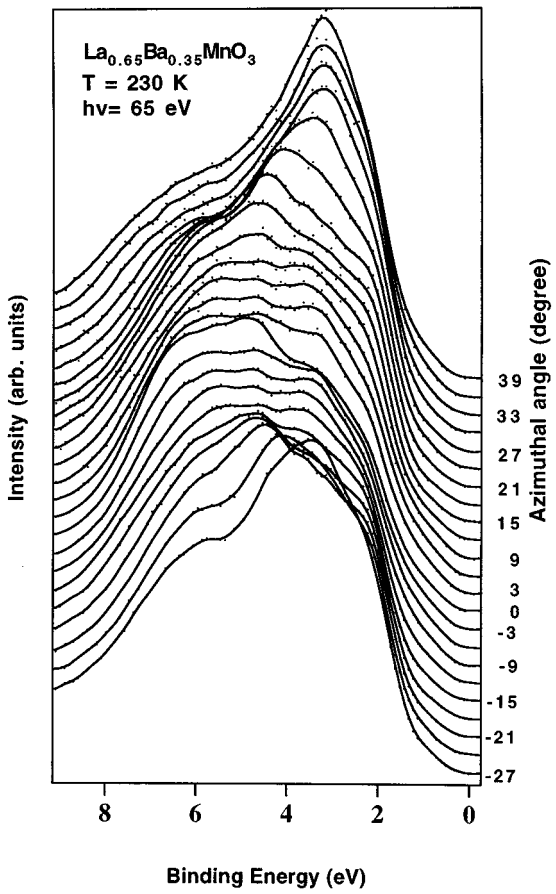

FIG. 11. Valence-band spectra of $La_{0.65}Ba_{0.35}MnO_3$ acquired at a photon energy of 65 eV along the Γ-X high-symmetry direction.

resonance edge). The increased intensity of this state with increasing emission angle observed for photon energies of 55 and 65 eV is characteristic of a surface state or resonance. Such behavior has been observed for the surface states of Cu(100) (Ref. 35) and Si(111).[36]

The dispersion of the bands of $La_{0.65}Ba_{0.35}MnO_3$ along the Γ-X symmetry direction are mapped out in Fig. 13. The

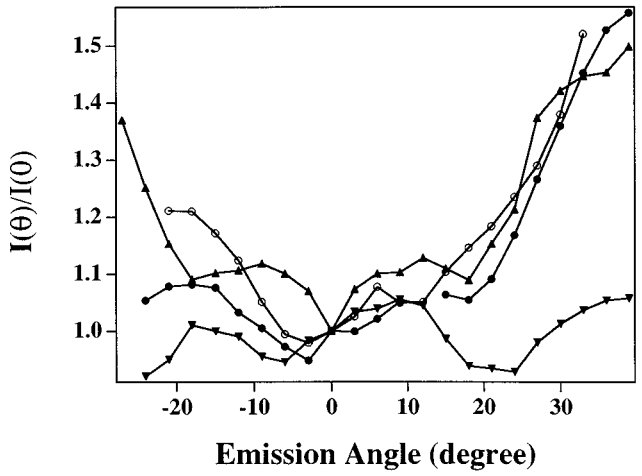

FIG. 12. The intensity of the 3.35-eV valence-band state of $La_{0.65}Ba_{0.35}MnO_3$ as a function of emission angle for photon energies of 45 eV (▼), 55 eV (▲), 65 eV (●) and (O).

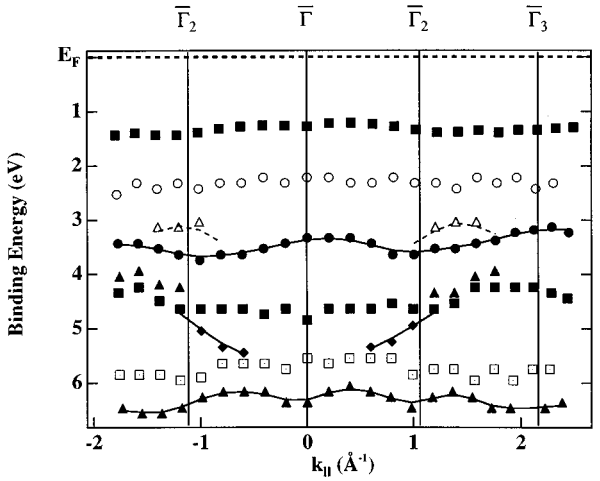

FIG. 13. The measured dispersion of the bands of $La_{0.65}Ba_{0.35}MnO_3$ along the Γ-X high-symmetry direction.

width of the band at 1.6 eV is approximately 250 meV. The bandwidth of the surface resonance at approximately 3.35-eV binding energy is visibly larger at 325 meV. Another very itinerant band is seen to disperse downward from a binding energy of 4.25 eV at Γ_2 to 5.5 eV halfway across the first zone, i.e., a bandwidth of 1.25 eV. The two bands at binding energies of 5.5 and 6.3 eV at the zone center have equivalent bandwidths of 350 meV along the Γ-X symmetry direction.

Based on the periodicity of the 5.5- and 6.3-eV bands, we have determined the zone edge to be at 1.15 $Å^{-1}$ from the zone center. This translates into a lattice vector of 5.46 Å, which is almost exactly the bulk lattice vector of $La_{0.65}Ca_{0.35}MnO_3$, and, within a small approximation, is roughly equivalent to that of $La_{0.65}Ba_{0.35}MnO_3$.[2]

In panel (a) of Fig. 14 the valence-band spectra of $La_{0.65}Ba_{0.35}MnO_3$ acquired with photon energies below (47 eV) and above (52 eV) the Mn 3p core-level edge are displayed. The difference curve between these two spectra shows the enhancement of the Mn-derived bands in the 0–3.5- and the 5–7-eV regions. This difference curve of $La_{0.65}Ba_{0.35}MnO_3$ is very similar to the difference curve of $La_{0.65}Ca_{0.35}MnO_3$ in panel (a) of Fig. 9, and demonstrates the consistency between the resonance behavior of these two systems.

The CIS spectra of $La_{0.65}Ba_{0.35}MnO_3$ [Fig. 14(b)] for an initial state 2.5 eV below the Fermi level exhibit the same characteristic resonance at the Mn 3p core-level edge observed for $La_{0.65}Ca_{0.35}MnO_3$. There is significantly more structure in the CIS spectra of $La_{0.65}Ba_{0.35}MnO_3$, in comparison to the CIS spectra of $La_{0.65}Ca_{0.35}MnO_3$ in Fig. 9. In particular there is the added structure at a photon energy of 58 eV. Deconvolution of the CIS spectrum of $La_{0.65}Ba_{0.35}MnO_3$ reveals the existence of a weaker secondary peak at a photon energy of 56 eV. The prominence of this secondary resonance feature of $La_{0.65}Ba_{0.35}MnO_3$ may be accentuated by the lower intensity of this resonance process, as compared to $La_{0.65}Ca_{0.35}MnO_3$.

It is this Mn 2p resonance that leads to some of the lineshape changes in the valence-band spectra of Fig. 6 with changes in photon energy. Thus, in addition to the effect of

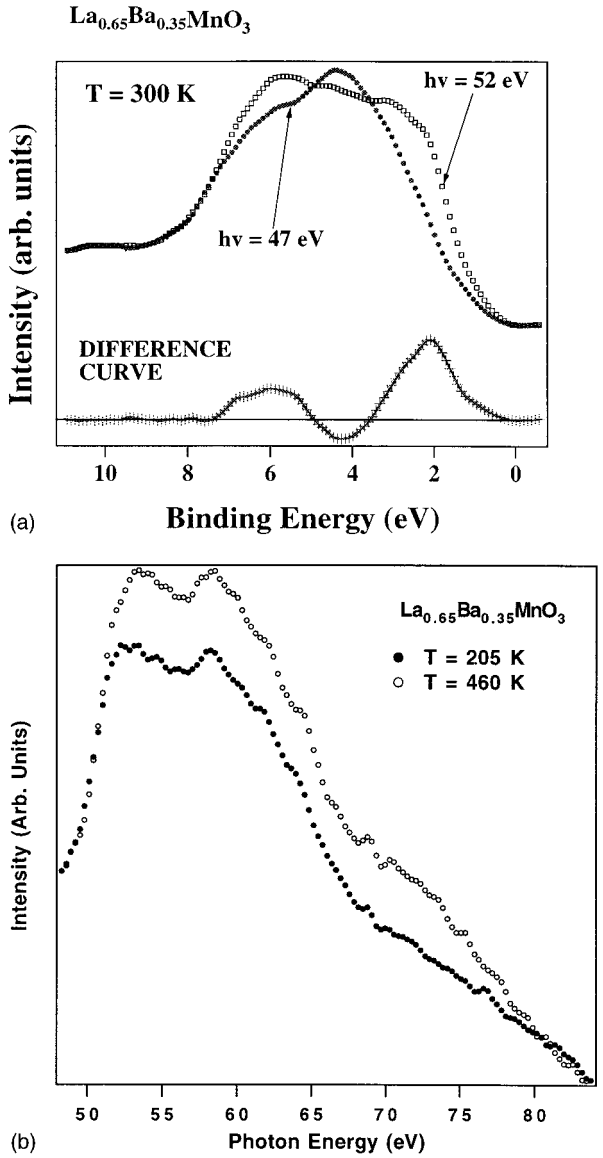

FIG. 14. (a) Valence-band spectra of $La_{0.65}Ba_{0.35}MnO_3$ acquired with photon energies of 47 eV (●) and 52 eV (□) at 300 K ($<T_c$). The difference curve for the two spectra is displayed below (+). (b) The resonance photoemission spectra of $La_{0.65}Ba_{0.35}MnO_3$ at 205 K (●) and 460 K (O), respectively, where the initial state is at a binding energy of 2.5 eV.

bulk band structure of some states of $La_{0.65}Ba_{0.35}MnO_3$, the Mn resonance leads to pronounced differences (as with $La_{0.65}Ca_{0.35}MnO_3$, seen in Fig. 9) in the spectra with changes in photon energy. Thus the spectra at 45 and 47 eV (below resonance) differ from other spectra of Fig. 6(b).

C. Temperature dependence of the valence band and resonance intensity of $La_{0.65}Ca_{0.35}MnO_3$ and $La_{0.65}Ba_{0.35}MnO_3$

1. $La_{0.65}Ca_{0.35}MnO_3$

Temperature-dependent changes in the valence-band structure of $La_{0.65}Ca_{0.35}MnO_3$ have been observed which correlate with the bulk transition temperature T_c.[37] In Fig. 15 the valence-band spectra of $La_{0.65}Ca_{0.35}MnO_3$ at temperatures above and below T_c are displayed. Below T_c, the state

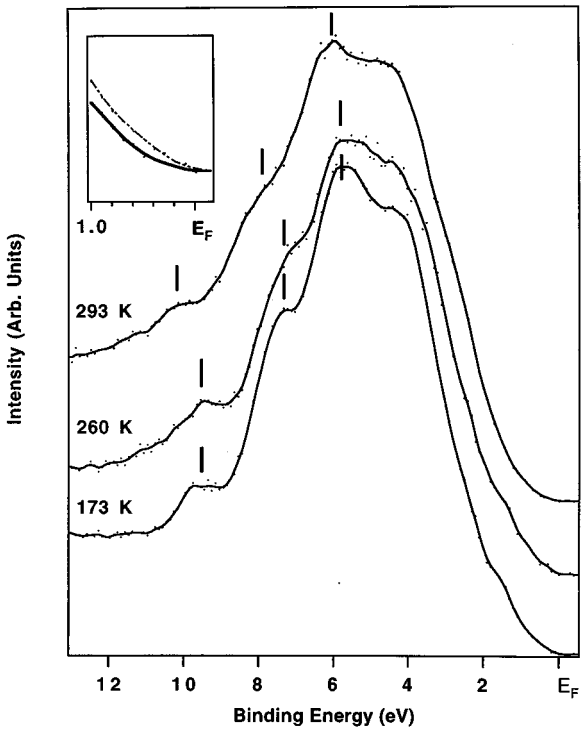

FIG. 15. Valence-band spectra of $La_{0.65}Ca_{0.35}MnO_3$ acquired at normal emission with a photon energy of 50 eV for various temperatures. The inset is an expanded view of the normalized spectra acquired at $T=293$ K (solid curve) and at $T=173$ K (dashed line) in the vicinity of the Fermi level. The bars are a guide to illustrate the shifts in the valence-band features with changes in temperature.

at 1.9 eV shifts toward the Fermi level. This shift was verified by Park *et al.*[34] The integrated density of states from a binding energy of 1.7 eV up to the Fermi level decreases continuously with increasing temperature, and correlates exactly with the coupled metallic/magnetic transition.[37] In addition to the shift of the band at 1.9 eV, the states at 7.7 and 9.5 eV also shift to lower binding energies (Fig. 15) with decreasing temperature.

These shifts in the occupied band structure are more easily seen by examining the band dispersion for $T<T_c$ in Fig. 8. While the bandwidths of the valence states ($W_{\max}=200$ meV) have not changed significantly from the room temperature measurements for $T<T_c$, the features initially at binding energies of 1.9 and 7.7 eV shift toward the Fermi level by 170 and 225 meV, respectively, while the features initially at 3.35 and 4.0 eV shift to higher binding energies by 260 and 125 meV, respectively. In contrast, the feature at 5.9 eV remains rigidly fixed.

The IPES spectra of $La_{0.65}Ca_{0.35}MnO_3$ were found to be temperature independent. We have attributed this to the reduced resolution of IPES, as compared to UPS. Consequently, our results do not rule out the possibility of temperature-dependent shifts of the unoccupied bands.

In addition to the temperature dependence of the binding energies of the valence states, temperature-dependent changes in the resonance process have also been observed. In panel (a) of Fig. 9, the valence-band spectra of $La_{0.65}Ca_{0.35}MnO_3$ acquired at photon energies of 47 eV (below the Mn $3p$ core-level edge) and at 52 eV (above the Mn

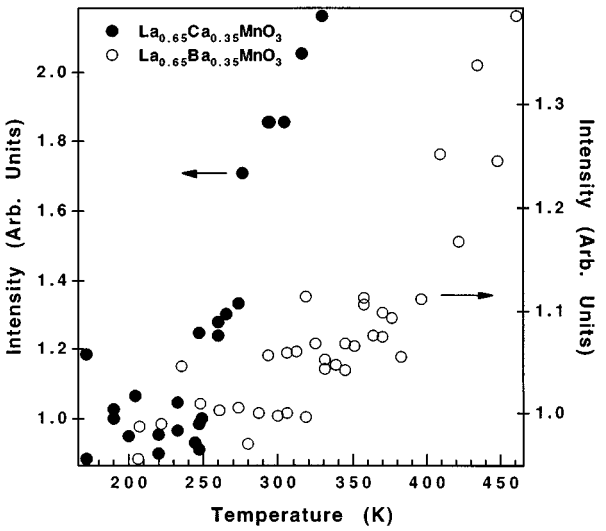

FIG. 16. The normalized integrated resonance photoemission intensity of $La_{0.65}Ca_{0.35}MnO_3$(●) and $La_{0.65}Ba_{0.35}MnO_3$ (O) as a function of temperature.

$3p$ core-level edge) for temperatures above and below the bulk transition temperature T_c. The resonance enhancement is significantly less for $T<T_c$, as compared to $T>T_c$. In panel (b) of Fig. 9, the CIS spectra of $La_{0.65}Ca_{0.35}MnO_3$ acquired for an initial state of 2.7 eV below the Fermi level acquired at $T>T_c$ and $T<T_c$. As expected, the CIS spectra also show the resonance onsets at the Mn $3p$ core-level edge, and that the resonance is quite intense for $T>T_c$. The temperature dependence of the resonance intensity as a function of temperature is displayed in Fig. 16. The intensity of the resonance increases by 120% from 170 to 320 K. A critical temperature of 260 K has been determined for the temperature dependence of the resonance process. This is equivalent to the bulk value for T_c.

2. $La_{0.65}Ba_{0.35}MnO_3$

The valence-band states of $La_{0.65}Ba_{0.35}MnO_3$ do not exhibit the temperature dependence observed for $La_{0.65}Ca_{0.35}MnO_3$. None of the valence state binding energies of $La_{0.65}Ba_{0.35}MnO_3$ shifted with changes in temperature. The dispersion of the bands $La_{0.65}Ba_{0.35}MnO_3$ are also temperature independent. As is the case for $La_{0.65}Ca_{0.35}MnO_3$, the IPES spectra of $La_{0.65}Ba_{0.35}MnO_3$ also did not exhibit temperature dependence.

The only observable spectroscopic temperature-dependent effect is the increase in the resonance intensity for $T>T_c$ displayed in Fig. 16. Like $La_{0.65}Ca_{0.35}MnO_3$, the resonance intensity of $La_{0.65}Ba_{0.35}MnO_3$ increases as the sample temperature is raised above T_c. The integrated resonance intensity of $La_{0.65}Ba_{0.35}MnO_3$ is plotted as a function of temperature in Fig. 16. The resonance intensity remains flat until approximately 330 K, at which point it begins to increase steadily with increasing temperature. This onset temperature corresponds very closely to the bulk transition temperature of 350 K. The intensity of the resonance $La_{0.65}Ba_{0.35}MnO_3$ across the metal-insulator transition changes by 40%.

V. DISCUSSION

A. Band assignments

Based on the polarization dependence, resonant enhancement, and a linearized muffin-tin orbital method. (LMTO) calculation of the valence band of $La_{0.50}Ca_{0.50}MnO_3$,[38] we have assigned the state at 1.9 eV in Fig. 7 to the Mn e_g band and the state at 3.0 eV to the Mn t_{2g} band. The state at 4.0 eV is strongly enhanced with p-polarized light, and is enhanced across the Mn $3p$ threshold, and therefore has large contributions from the Mn $3d_{z^2\text{-}r^2}$ orbital, i.e., $\Delta_1(a_1)$ character assuming C_{4v} symmetry for the surface. The state at 5.9 eV is mainly p_z in character, and is associated with the O $2p$ bands. This assignment is consistent with the temperature independence of this band in Fig. 8. Based on the LMTO calculation, we have assigned the state at 7.7 eV to a Mn t_{2g}–O $2p$ band. There are two possible origins of the state at 9.54 eV. One is that it is a σ-bonding state arising from Mn-O $pd\sigma$ hybridization (Δ_5 character for the surface or an t_{2g} orbital for bulk symmetry). Alternatively, it could be a satellite state, which have been observed for transition-metal oxides[39] arising from many-body effects.[40] Our band assignments are consistent with a number of other calculations for Ca concentrations ranging from $x=0$ to 1.[40,41]

We do not expect the band assignments of $La_{0.65}Ba_{0.35}MnO_3$ to differ significantly from $La_{0.65}Ca_{0.35}MnO_3$. Based on LMTO bulk band structure calculations of $La_{0.75}Ba_{0.25}MnO_3$,[26] we have made the following assignments for the valence bands of $La_{0.65}Ba_{0.35}MnO_3$ in Fig. 13: the state at 1.27 eV at the zone center is assigned to the Mn e_g band, and the states at 2.5 and 3.35 eV are assigned to the Mn t_{2g} bands. These assignments are consistent with the resonance enhancement of these states across the Mn $3p$ edge in Fig. 14(a). The band at 3.0 eV between the second and third zone centers in Fig. 5 is tentatively assigned to a bulk Mn t_{2g} band. The origin of this band is difficult to determine with a high degree of confidence, since it is nearly always degenerate with the t_{2g} band at 3.35 eV. The fact that the band at 4.8 eV in Fig. 14(a) is not enhanced at a photon energy of 52 eV indicates that it has very little Mn character and is predominantly oxygen $2p$ in character, similar to the 5.9-eV state of $La_{0.65}Ca_{0.35}MnO_3$. The states at 5.5 and 6.3 eV at the zone center in Fig. 13 show strong enhancement across the Mn resonance [see Fig. 14(a)]. We therefore assign these states of $La_{0.65}Ba_{0.35}MnO_3$ to the high-binding-energy components of the Mn t_{2g} symmetry band which hybridize with the O $2p$ states. This is consistent with the LMTO calculations of $LaMnO_3$ in Ref. 38 and the local-density-approximation calculations of $LaMnO_3$ by Satpathy, Poporic, and Vukajlovic.[40]

The IPES spectrum of $La_{0.65}Ca_{0.35}MnO_3$ in Fig. 10 can be broken down into two regions. The first region is the broad shoulder between the Fermi level and approximately 3 eV, and based on calculations in Ref. 40 for $LaMnO_3$, we have assigned this region of the unoccupied density of states to the minority components of the e_g and t_{2g} bands, respectively, with the e_g band at the conduction-band minimum. This is consistent with assignments made by Park *et al.*[34] from x-ray-adsorption spectroscopy of $LaMnO_3$ and $CaMnO_3$.

The second region is a broad feature centered around 7.0 eV, which we assigned to unoccupied states of largely La and Ca $5d$ character.[41]

The same assignments of the unoccupied bands of $La_{0.65}Ca_{0.35}MnO_3$ should hold true for $La_{0.65}Ba_{0.35}MnO_3$, with the exception that the broad feature at 7.0 eV in Fig. 10 is now composed of unoccupied La and Ba $5d$ states. This unoccupied band of $La_{0.65}Ba_{0.35}MnO_3$ is much broader than the corresponding band of $La_{0.65}Ca_{0.35}MnO_3$. This is probably due to extended hybridization between the La and Ba bands with unoccupied O $2p$ and Mn t_{2g} bands, and is consistent with the larger bandwidths of the states of $La_{0.65}Ba_{0.35}MnO_3$, relative to $La_{0.65}Ca_{0.35}MnO_3$.

B. Surface properties

The issue of surface states, or surface resonances, is very important, and must be considered when attempting to base conclusions about the bulk properties from surface spectroscopies, in particular, photoemission. Liu and Klemm[42] proposed the existence of two-dimensional states confined to the surface of high-temperature superconductors (HTSC's). Furthermore, they suggest that these states do not reflect the behavior of the bulk due to vanishing spectral weight at specific points in the surface Brillouin zone. Their conclusions are supported by changes in the apparent photoemission gap in HTSC materials due to surface contamination which have been observed using ARUPS.[43]

The suppression of the $La_{0.65}Ba_{0.35}MnO_3$ t_{2g} band at 3.35 eV with CO contamination and disorder (Fig. 4) supports our conclusion that this state is localized at the surface-vacuum interface. While the band at 1.27 eV does appear to be localized at the surface-vacuum interface, we will refrain from identifying this band as a surface resonance until further information can be obtained. The 3.35-eV state cannot be considered a surface state because it does not reside in a gap of the projected bulk bands,[26] and therefore must be defined as a surface resonance. This is consistent with the absence of dispersion of this state normal to the surface. Additionally, the increased intensity of this state with emission angle in Fig. 12 is also characteristic of the surface localization. Taken together, these results conclusively identify the t_{2g} band at 3.35 eV, and possibly the e_g band at 1.27 eV, as surface resonances.

The existence of a Mn-derived surface resonance strongly argues in favor of Mn-O surface termination. Conduction in these materials is through an e_g band localized within the Mn-O planes; therefore, Mn-O surface termination may explain why we obtain such excellent agreement between the value of T_c based on CIS measurements and the bulk transport measurements. Because the surface resonances are resonances and *not* true surface states,[26] coupling with the bulk is reasonable. The wave function of the surface electronic structure is not localized entirely at the surface. The equally good agreement between the photoemission results of $La_{0.65}Ca_{0.35}MnO_3$ (Ref. 37) with the bulk transport measurements further suggests that, in general, the Mn-O plane is the favorable form of surface termination of this family of perovskites.

Additional support for Mn-O surface termination is obtained from the IPES spectra in Figs. 5 and 10. IPES is a technique which is even more surface sensitive than photoemission. The strong spectral weight of the minority Mn bands at the conduction-band minimums of $La_{0.65}Ca_{0.35}MnO_3$ and $La_{0.65}Ba_{0.35}MnO_3$ in Fig. 10 argues against surface termination by the La-O planes. If the surfaces were terminated with La-O planes, strong contributions from the Mn minority bands would not be expected due to localization of the Mn-derived bands below the surface, and electron mean free path arguments. Further, the $4f$ unoccupied states of La and Ba would dominate the IPES spectra, which they do not. This is consistent with the suppression of the unoccupied e_g and t_{2g} bands of $La_{0.65}Ba_{0.35}MnO_3$ in Fig. 5 with CO adsorption.

The existence of surface resonance(s) of $La_{0.65}Ba_{0.35}MnO_3$ indicates that the electronic structure of the surface may differ from the bulk, and casts some doubt on the ability to probe the gap of these materials, as we have noted previously. (The dominant role played by changes in the screening parameter—discussed later—casts further doubt on the effectiveness of photoemission in determining the gap.) An accurate determination of the gap could be seriously underestimated with surface contamination, or surface disorder. Ultraviolet photoemission is a tool which can provide useful information about these systems, yet its limitation must be considered when examining phenomena such as gap changes on the order of 50 meV. Even with cleaved samples, it may be difficult to obtain high quality defect-free surfaces which do not significantly alter the apparent width of the gap. The strength of UPS for studying the perovskites appears to lie in the areas of band structure determination and local screening.

The sputtered spectrum in Fig. 4 raises the issue of surface order and how disorder modifies the electronic structure of the perovskites. It has been reported that the fingerprint of surface contamination for $La_{1-x}Sr_xMnO_3$ is a pronounced spectral feature at, or near, a binding energy of 10 eV.[31] While spectra displaying this feature were not shown in Ref. 31, we suspect that they are very similar to the spectrum of the sputtered surface of $La_{0.65}Ba_{0.35}MnO_3$ in Fig. 4. In Ref. 31, the surface was considered to be clean, where cleaning was achieved by filling, once the 10-eV feature was no longer observed. Such a surface may be highly disordered and not dissimilar from the sputtered surface characteristic of Fig. 4.

For many compound oxide materials, uniform sputtering of the different elements is very unlikely. In many cases, one element is preferentially removed from the surface over another. In cases where O is preferentially sputtered, or depleted, from the surface of a transition-metal oxide, a well-defined density of states is often observed at the Fermi level, i.e., a metal-rich surface. A very good example of this type of behavior is TiO_2.[44] The valence-band spectrum of the sputtered surface of $La_{0.65}Ba_{0.35}MnO_3$ in Fig. 4 actually exhibits a decrease in the density of states at and near the region of the Fermi level. Preferential sputtering from the surface of $La_{1-x}Ca_xMnO_3$ has been observed by others.[45]

C. Band structure, screening, and metallicity

To date, the majority of the electronic studies of the perovskites have focused on the structure of the valence

band,[31,33,46–48] but only a few have explored the dispersive behavior of the valence states.[26,38] The band structure results of $La_{0.65}Ca_{0.35}MnO_3$ and $La_{0.65}Ba_{0.35}MnO_3$ presented in Sec. III clearly demonstrate that the electronic structure of these very similar materials are dramatically different.

The measured band dispersion $La_{0.65}Ca_{0.35}MnO_3$ in Fig. 8 is characteristic of a flat-band system (bandwidths less than 200 meV) and is indicative of the localized nature of the valence electrons. This localized character is consistent with the susceptibility of this system to dynamic and static Jahn-Teller distortions.[16,17] The shift of the e_g band of $La_{0.65}Ca_{0.35}MnO_3$ toward the Fermi level (see Fig. 15) as the system passes from the paramagnetic-insulating phase to the ferromagnetic-metallic phase agrees with the band shifts predicted for a Jahn-Teller displacement of a Mn^{3+} ion in an octahedral coordination.[49] The increased exchange splitting between the e_g and t_{2g} bands across the transition is also consistent with Jahn-Teller distortions. The change in the density of states in the neighborhood of the Fermi level as a function of temperature, i.e., the shift of the e_g band correlates with the bulk properties,[37] and demonstrates the correlation of the band shifts with the bulk properties.

Care must be taken when drawing conclusions about structural distortions based on band shifts without taking into account final-state effects. Oxides are highly susceptible to final-state effects, and a flatband system like $La_{0.65}Ca_{0.35}MnO_3$ is especially susceptible. However, an examination of Fig. 8 shows that not all of the bands shift in the same direction across the transition. The Mn e_g band and the component of the t_{2g} band with $3d_{xz}$, $3d_{yz}$ orbital character at 7.7 eV shift toward the Fermi level as the system passes from the insulating phase to the metallic phase. In contrast, the component of the Mn t_{2g} band at 3.0 eV and the Mn-O band at 4.0 eV shift to higher binding energies. If the shift of the e_g band is due to final-state effects, then all of the bands should shift in the same direction. So we can conclude that this shift of the e_g band is, in part, due to initial-state effects, e.g., Jahn-Teller distortions and other effects.

The dispersion of the bands of $La_{0.65}Ba_{0.35}MnO_3$ is characteristic of a demonstrably different electronic structure. The valence-band spectra of $La_{0.65}Ba_{0.35}MnO_3$ along the $\overline{\Gamma}$-$\overline{X}$ symmetry line in Fig. 11 illustrates the dispersive character of the valence states. As with $La_{0.65}Ca_{0.35}MnO_3$, the e_g band of $La_{0.65}Ba_{0.35}MnO_3$ at 1.6 eV is flat, with a bandwidth which is $\leqslant$ 200 meV. The t_{2g} band at a binding energy of 3.35 eV is also fairly localized, but has a slightly larger bandwidth of 250 meV. The flatband character of the e_g and t_{2g} bands of $La_{0.65}Ca_{0.35}MnO_3$ and $La_{0.65}Ba_{0.35}MnO_3$ is consistent with band-structure calculations for these two systems.[26,41] However, the bands of $La_{0.65}Ba_{0.35}MnO_3$ in the 4–8-eV region in Fig. 13 are much more itinerant, where one band (5.5 eV at $\overline{\Gamma}$) disperses by as much as 1.25 eV. The corresponding bands of $La_{0.65}Ca_{0.35}MnO_3$ disperse very little.

The itinerant character of these bands suggest that the Mn-O hybridization is much greater for $La_{0.65}Ba_{0.35}MnO_3$, relative to $La_{0.65}Ca_{0.35}MnO_3$. Due to the large ionic radius of Ba, as compared to Ca, a greater Hückel orbital overlap is expected. The increased overlap will delocalize the Mn states through increased hybridization with the O bands. Recently it has been shown that modifications of the Mn-O-Mn bond angles lowered the transition temperature of $La_{1-y-x}Y_yCa_xMnO_3$.[19,20] It is argued that changes in Mn-O-Mn bond angles can increase the coupling (B) between moving carriers and localized spins.[50] This appears to be consistent with pressure-induced shifts of T_c of $La_{1-x}Sr_xMnO_3$.[9] This coupling (B) is related to the nearest-neighbor spin coupling (J) and the bandwidths (W): $B \approx J/W$.[50,51] According to this relationship, the coupling can be modified by either changing J or W. Fontcuberta *et al.*[19] argued that T_c decreases as the coupling B increases. This argument appears to be consistent with the measured bandwidths of $La_{0.65}Ca_{0.35}MnO_3$ ($W < 200$ meV; $T_c = 260$ K) and $La_{0.65}Ba_{0.35}MnO_3$ (250 meV $< W <$ 1.25 eV; $T_c = 320$ K), where the higher critical temperature of $La_{0.65}Ba_{0.35}MnO_3$ is a consequence of the larger ionic radius of Ba (1.35 Å) which increases the Mn-O-Mn bond angles, relative to Ca (0.99 Å).

It is worth noting that the extended nature of the states of $La_{0.65}Ba_{0.35}MnO_3$ are manifested in the structure and energy range of the resonance in the CIS spectra in Fig. 14(b). The resonance observed for $La_{0.65}Ca_{0.35}MnO_3$ in Fig. 9(b) only extends from 47 to 62 eV, and is fairly smooth without any discernible structure. In contrast, the resonance of $La_{0.65}Ba_{0.35}MnO_3$ in Fig. 14(b) not only extends over a greater photon range (47–80 eV), but also has a pronounced structure. This added structure appears as a peak in the spectra at 58 eV. In addition to this peak, there appears to be some fine structure between 60 and 65 eV in the form of shoulders, but further interpretation would be speculative at best. We hypothesis that this richer structure is due to the extended nature of the occupied states of $La_{0.65}Ba_{0.35}MnO_3$, and that this results in enhanced coupling to the unoccupied states. We believe that this explanation also accounts for the broad ($\Delta E \sim 10$ eV) peak centered at 72.5 eV in Fig. 14(b). The observance of the second peak at 58 eV in Fig. 14(b) is similar to a peak observed in the resonance spectra of TiO_2, where the strength of this peak was related to the degree of hybridization between Ti $3d$ and O $2p$ states.[44] When the TiO_2 surface was oxygen reduced and the Ti-derived states became more localized, the intensity of this peak diminished. This is consistent with the localized character of the bands of $La_{0.65}Ca_{0.35}MnO_3$ and explains why this structure is absent from the CIS spectra in Fig. 9(b).

The larger bandwidths of the Mn-O bands of $La_{0.65}Ba_{0.35}MnO_3$ should be manifested in changes in electron-phonon interactions and Coulombic interactions (U). This leads us to the issue of whether $La_{0.65}Ba_{0.35}MnO_3$ exhibits a metal-insulator transition, or remains metallic. The phase diagram of $La_{0.65}Ca_{0.35}MnO_3$ is fairly well known.[3,52] Clearly, $La_{1-x}Sr_xMnO_3$: $x = 0.35$ exhibits a metal-insulator transition with increasing temperature. Yet, it has been demonstrated that $La_{1-x}Sr_xMnO_3$: $x = 0.30$ does not exhibit a metal-insulator transition, but remains metallic as the system traverses the ferromagnetic-paramagnetic transition.[4,7] One of the signatures of the metal-metal phase of $La_{0.70}Sr_{0.30}MnO_3$ is a plateau rather than a decreasing resistivity once the maximum resistivity has been attained.[4] Such a plateau is observed for $La_{0.65}Ba_{0.35}MnO_3$ in Fig. 2, and in Fig. 2(b) in Ref. 1.

As previously stated, the band dispersion and binding energies of the states of $La_{0.65}Ba_{0.35}MnO_3$ are temperature independent. Taken in conjunction with the enhanced dispersion of the bands of $La_{0.65}Ba_{0.35}MnO_3$ over $La_{0.65}Ca_{0.35}MnO_3$, these results argue against $La_{0.65}Ba_{0.35}MnO_3$ exhibiting dynamic Jahn-Teller distortions. To our knowledge, dynamic Jahn-Teller distortions have not been observed for $La_{0.65}Ba_{0.35}MnO_3$. This may explain the apparent metallicity of $La_{0.65}Ba_{0.35}MnO_3$ on either sides of the magnetic transition. This issue is still unclear, and will need to be explored in greater detail.

The screening parameter, in turn, is related to the Mn $3p \rightarrow \varepsilon d$ resonance intensity (I) obtained from CIS,[53] and given by the relationship,

$$\{I(T)/I_m\}^2 \propto \{l_s(T)/l_m\}^{-2},$$

or

$$I(T) \propto 1/l_s(T),$$

where I_m and l_m are the resonance intensity and the screening parameter in the metallic phase, respectively, and $I_s(T)$ is the temperature-dependent screening parameter. The temperature-dependent change of the resonance intensity across T_c should give a measure of the temperature dependence of the screening parameter. In the metallic phase the resonance intensity will be small, i.e., $I_s(T<T_c) \simeq I_m$, relative to the insulating phase where $I_s(T>T_c) > I_m$, i.e., strong localization.

The resonance intensity of the e_g band of $La_{0.65}Ca_{0.35}MnO_3$ increases by 120% across the transition (see Fig. 16). This resonance effect is a combined probe of the screening of the Mn e_g band, as well as the collective medium, i.e., the screening parameter. We can conclude from the large change of the resonance intensity that a reduction in the screening parameter takes place across the metal-insulator transition. Not only are the electrons in the e_g band localized, but the ability of the collective medium to adequately screen the Coulombic binding of the core exciton is also diminished in the insulating phase.

Within the same temperature range, the resonance of $La_{0.65}Ba_{0.35}MnO_3$ increased by only 40% (see Fig. 16). This indicates that for $La_{0.65}Ba_{0.35}MnO_3$, the screening parameter does not dramatically change across the metal-insulator transition in quite as dramatic a fashion as in $La_{0.65}Ca_{0.35}MnO_3$. Another way of stating this is that the screening within $La_{0.65}Ba_{0.35}MnO_3$ is very efficient (screening lengths are very short), relative to $La_{0.65}Ca_{0.35}MnO_3$, both above and below the coupled metallic-magnetic transition. The resonance behavior of $La_{0.65}Ba_{0.35}MnO_3$ as a function of temperature is more consistent with a metallic–ferromagnetic–metallic-paramagnetic transition. We suggest that the greater electron itinerancy in $La_{0.65}Ba_{0.35}MnO_3$ may suppress dynamic Jahn-Teller distortions.

Clearly, the resonance behavior reflects the changes in the localization of the electrons within these systems due to magnetic disorder, since the resistivity can be suppressed with sufficiently large fields [see Figs. 1(a) and 2]. If the electron charge involved in screening becomes localized by magnetic disorder, the dynamic dielectric response of the collective medium becomes slower, and the medium will no longer respond quickly to changes in local interactions and coupling.

The larger negative magnetoresistance of $La_{0.65}Ca_{0.35}MnO_3$, as compared to $La_{0.65}Ba_{0.35}MnO_3$, is reflected in the 120% change in the resonance intensity across the metal-insulator transition, relative to 40% for $La_{0.65}Ba_{0.35}MnO_3$. This leads us to speculate that $La_{0.65}Ba_{0.35}MnO_3$ exhibits a dynamic Jahn-Teller distortion because of the localized nature of its bands both above and below T_c. Conversely, we suggest that $La_{0.65}Ba_{0.35}MnO_3$ may not experience dynamic Jahn-Teller distortions due to the delocalized nature of its bands.

VI. SUMMARY

We have examined the electronic band structure of $La_{0.65}Ca_{0.35}MnO_3$ and $La_{0.65}Ba_{0.35}MnO_3$ both above and below the coupled magnetic-metallic phase transition. We have found that the valence-band structure of $La_{0.65}Ba_{0.35}MnO_3$ is very sensitive to surface conditions. A surface resonance (or resonances) of $La_{0.65}Ba_{0.35}MnO_3$ has been observed. The surface localization of this state has been verified by the absence of dispersion perpendicular to the surface, as well as from surface modifications (CO adsorption and sputtering) which attenuate the signal of this state (or states). The existence of a surface resonance (or resonances) demonstrates that large contributions to the valence band originate from the surface, and that care must been taken when interpreting bulk phenomena based on valence-band photoemission.

The bands of $La_{0.65}Ca_{0.35}MnO_3$ are highly localized, with bandwidths of less than 200 meV. Temperature-dependent shifts of the e_g and t_{2g} bands of $La_{0.65}Ca_{0.35}MnO_3$ have been observed, and appear to correlate with the predicted band shifts associated with dynamic Jahn-Teller distortions. The screening parameter of $La_{0.65}Ca_{0.35}MnO_3$ changes dramatically across the coupled magnetic-metallic phase transition, and is a signature of changes in the local screening of the Mn ions. On the other hand, we found the bands of $La_{0.65}Ba_{0.35}MnO_3$ to be highly itinerant. One bulk band was observed to disperse by as much as 1.25 eV. Unlike $La_{0.65}Ca_{0.35}MnO_3$, the bands of $La_{0.65}Ba_{0.35}MnO_3$ neither shift, nor do their dispersions change, across the magnetic phase transition. Changes in the screening parameter of $La_{0.65}Ba_{0.35}MnO_3$ were observed, but were found to be less dramatic than for $La_{0.65}Ca_{0.35}MnO_3$.

Upon comparing these two systems, we concluded that the shifts of the e_g and t_{2g} bands of $La_{0.65}Ca_{0.35}MnO_3$ are a consequence of large changes in the screening parameter of this material across the coupled magnetic-metallic phase transition, and that the existence of Jahn-Teller distortions is a consequence, not a cause. These band shifts do not occur for $La_{0.65}Ba_{0.35}MnO_3$, because the screening within this system is more efficient. Based on our findings, we believe that $La_{0.65}Ba_{0.35}MnO_3$ does not exhibit a metal-insulator transition, but remains metallic on both sides of the ferromagnetic-paramagnetic transition.

ACKNOWLEDGMENTS

This work was supported by NSF Grant Nos. DMR-92-21655, DMR-94-96131, OSR-9255225, and the Atomic Technology Partnership (ATP) in Japan. This work was partially based on research conducted at the Synchrotron Radiation Center which is supported by the NSF under Award No. DMR-95-31009.

*Permanent address: The Department of Physics, Engineering and Physics Bldg., The University of ldaho, Moscow, ID 83844-2341.

†Permanent address: The Department of Physics, 203 South College, The University of Tennessee, Knoxville, TN 37996-1200.

[1] R. von Helmolt, J. Wecker, B. Holzapfel, L. Schultz, and K. Samwer, Phys. Rev. Lett. **71**, 2331 (1993); R. von Helmolt, J. Wecker, T. Lorenz, and K. Samwer, Appl. Phys. Lett. **67**, 2093 (1995); R. von Helmolt, J. Wecker, K. Samwer, and K. Bärner, J. Magn. Magn. Mater. **151**, 411 (1995).

[2] Ken-ichi Chahara, T. Ohno, M. Kasai, and Y. Kozono, Appl. Phys. Lett. **63**, 1990 (1993).

[3] H. L. Ju, C. Kwon, Qi Li, R. L. Greene, and T. Venkatesan, Appl. Phys. Lett. **65**, 2108 (1994).

[4] Y. Tokura, A. Urushibara, Y. Moritomo, T. Arima, A. Asamitsu, G. Kido, and N. Furukawa, J. Phys. Soc. Jpn. **63**, 3931 (1994).

[5] M. R. Lees, J. Barratt, G. Balakrishnan, D. McK. Paul, and M. Yethiraj, Phys. Rev. B **52**, 14 303 (1995).

[6] M. F. Hundley, M. Hawley, R. H. Heener, Q. X. Jia, J. J. Neumeier, J. Tesmer, J. D. Thompson, and X. D. Wu, Appl. Phys. Lett. **67**, 860 (1995).

[7] A. Urishibara, Y. Moritomo, T. Arima, A. Asamitsu, G. Kido, and Y. Tokura, Phys. Rev. B **51**, 14 103 (1995); Y. Tokura, Y. Tomioka, H. Kuwahara, A. Asamitsu, Y. Moritomo, and M. Kasai, J. Appl. Phys. **79**, 5288 (1996).

[8] R. D. Sánchez, J. Rivas, C. Vázquez-Vázquez, A. López-Quintela, M. T. Causa, M. Tovar, and S. Oseroff, Appl. Phys. Lett. **68**, 134 (1996); G.-Q. Gong, C. Canedy, G. Xiao, J. Sun, A. Gupta, and W. Gallagher, *ibid*. **67**, 1783 (1995); A. Gupta, T. R. McGuire, P. R. Duncombe, M. Rupp, J. Z. Sun, W. J. Gallagher, and G. Xiao, *ibid*. **67**, 3494 (1995).

[9] Y. Moritomo, A. Asamitsu, and Y. Tokura, Phys. Rev. B **51**, 16 491 (1995).

[10] R. Mahendiran, S. K. Tiwary, A. K. Raychaudhuri, T. V. Ramakrishnan, R. Mahesh, N. Rangavittal, and C. N. R. Rao, Phys. Rev. B **53**, 3348 (1996).

[11] H. Kawano, R. Kajimoto, M. Kubota, and H. Yoshizawa, Phys. Rev. B **53**, 2202 (1996).

[12] G. H. Jonker and J. H. van Santen, Physica **16**, 337 (1950).

[13] J. H. van Santen and G. H. Jonker, Physica **16**, 599 (1950).

[14] C. Zener, Phys. Rev. **82**, 403 (1951); J. B. Goodenough, *ibid*. **100**, 564 (1955).

[15] A. J. Millis, P. B. Littlewood, and B. I. Shraiman, Phys. Rev. Lett. **74**, 5144 (1995).

[16] P. G. Radaelli, D. E. Cox, M. Marezio, S.-W. Cheong, P. E. Schiffer, and A. P. Ramirez, Phys. Rev. Lett. **75**, 4488 (1995).

[17] P. Dai, Jiandi Zhang, H. A. Mook, S.-H. Liou, P. A. Dowben, and E. W. Plummer, Phys. Rev. B **54**, R3694 (1996); Solid State Commun. (to be published).

[18] M. McCormack, S. Jin, T. H. Tiefel, R. M. Fleming, J. M. Philips, and R. Ramesh, Appl. Phys. Lett. **64**, 3045 (1994).

[19] J. Fontcuberta, B. Martínez, A. Seffar, S. Pinol, J. L. García-Muñoz, and X. Obradors, Phys. Rev. Lett. **76**, 1122 (1996).

[20] M. R. Ibarra, P. A. Algarabel, C. Marquina, J. Blasco, and J. García, Phys. Rev. Lett. **75**, 3541 (1996); A. Maignan, C. Simon, V. Caignaert, and B. Raveau, J. Appl. Phys. **79**, 7891 (1996).

[21] P. A. Dowben, D. LaGraffe, and M. Onellion, J. Phys. Condens. Matter **1**, 6571 (1989).

[22] P. W. Erdmann and E. C. Zipf, Rev. Sci. Instrum. **53**, 235 (1982).

[23] V. E. Henrich, G. Dresselhaus, and H. J. Zeiger, Phys. Rev. B **17**, 4908 (1978).

[24] Neal D. Shinn, Phys. Rev. B **38**, 12248 (1988).

[25] R. J. Lad and V. E. Henrich, J. Vac. Sci. Technol. A **6**, 781 (1988).

[26] C. Waldfried, D. N. Mcllroy, S.-H. Liou, R. Sabirianov, S. S. Jaswal, and P. A. Dowben, J. Phys. Condens. Matter (to be published).

[27] P. D. Johnson, D. A. Wesner, J. W. Davenport, and N. V. Smith, Phys. Rev. B **30**, 4860 (1984).

[28] S. L. Hulbert, Xiaohe Pan, and P. D. Johnson, Phys. Rev. B **35**, 7710 (1987).

[29] N. B. Brookes, A. Clarke, and P. D. Johnson, Phys. Rev. Lett. **63**, 2764 (1989).

[30] J. W. Allen, in *Synchrotron Radiation Research: Advances in Surface and Interface Science, Vol. 1: Techniques*, edited by R. Z. Bachrach (Plenum, New York, 1992); R. Bruhn, B. Sonntag, and H. W. Woff, Phys. Lett. A **69**, 9 (1978).

[31] T. Saitoh, A. E. Bocquet, T. Mizokawa, H. Namatame, A. Fujimori, M. Abbate, Y. Takeda, and M. Takano, Phys. Rev. B **51**, 13 942 (1995).

[32] R. J. Lad and V. E. Henrich, Phys. Rev. B **38**, 10 860 (1988).

[33] A. Chainani, M. Mathew, and D. D. Sarma, Phys. Rev. B **47**, 15 397 (1993).

[34] J.-H. Park, C. T. Chen, S.-W. Chenog, W. Bao, G. Meigs, V. Charkarian, and Y. U. Idzerda, J. Appl. Phys. **79**, 4558 (1996); Phys. Rev. Lett. **76**, 4215 (1996).

[35] S. C. Wu, C. K. C. Lok, J. Sokolov, J. Quinn, Y. S. Li, D. Tain, and F. Jona, Phys. Rev. B **39**, 13 218 (1989).

[36] M. M. Traum, J. E. Rowe, and N. E. Smith, J. Vac. Sci. Technol. **12**, 298 (1975).

[37] D. N. Mcllroy, Jiandi Zhang, S.-H. Liou, and P. A. Dowben, Phys. Lett. A **207**, 367 (1995).

[38] Jiandi Zhang, D. N. Mcllroy, P. A. Dowben, S.-H. Liou, R. F. Sabirianov, and S. S. Jaswal, Solid State Commun. **97**, 39 (1996).

[39] W. P. Ellis, A. M. Boring, J. W. Allen, L. E. Cox, R. D. Cowan, B. B. Pate, A. J. Arko, and I. Lindau, Solid. State Commun. **72**, 725 (1989).

[40] S. Satpathy, Z. S. Popovic', and F. R. Vukajlovic', Phys. Rev. Lett. **76**, 960 (1996).

[41] W. E. Pickett and D. J. Singh, Europhys. Lett. **32**, 759 (1995); Phys. Rev. B **53**, 1146 (1996); **53**, 1146 (1996).

[42] S. H. Liu and R. A. Klemm, Phys. Rev. Lett. **73**, 1019 (1994).

[43] Z.-X. Shen, D. S. Dessau, B. O. Wells, D. M. King, W. E. Spicer, A. J. Arko, D. Marshall, L. W. Lombardo, A. Kapitulnik, P. Dickinson, S. Doniach, J. DiCarlo, A. G. Loeser, and C. H. Park, Phys. Rev. Lett. **70**, 1553 (1993).

[44] Z. Zhang, S.-P. Jeng, and V. E. Henrich, Phys. Rev. B **43**, 12 004 (1991).

[45] Y. U. Idzerda (private communication).

[46] A. Chainani, M. Mathew, and D. D. Sarma, Phys. Rev. B **46**, 9976 (1992).

[47] D. D. Sarma, N. Shanthi, S. R. Krishnakumar, T. Saitoh, T. Mizokawa, A. Sekiyama, K. Kobayashi, A. Fujimori, E. Weschke, R. Meier, G. Kaindl, Y. Takeda, and M. Takano, Phys. Rev. B **53**, 6873 (1996).

[48] M. Abbate, F. M. F. de Groot, J. C. Fuggle, A. Fujimori, O. Strebel, F. Lopez, M. Domke, G. Kaindl, G. A. Sawatzky, M. Takano, Y. Takeda, H. Eisaki, and S. Uchida, Phys. Rev. B **46**, 4511 (1992).

[49] J. M. D. Coey, M. Viret, L. Ranno, and K. Ounadjela, Phys. Rev. Lett. **75**, 3910 (1995).
[50] J. Inoue and S. Maekawa, Phys. Rev. Lett. **74**, 3407 (1995).
[51] N. Furukawa, J. Phys. Soc. Jpn. **63**, 3214 (1994).
[52] A. P. Ramirez, P. Schiffer, S.-W. Cheong, C. H. Chen, W. Bao, T. T. M. Palstra, P. L. Gammel, D. J. Bishop, and B. Zegarski, Phys. Rev. Lett. **76**, 3188 (1996).
[53] Dongqi Li, Jiandi Zhang, Sunwoo Lee, and P. A. Dowben, Phys. Rev. B **45**, 11 876 (1992).